Spectrally Adaptable Compressive Sensing Imaging System

Quarterly Progress Report to the Office of Naval Research
Surveillance Technology Program

Contract number: NOOO14-1O-C-0 199
For period ending: June, 2010
Submitted by the University of Delaware
July 15, 2010

Submitted to:

Dr. Michael Duncan, Program Officer
Electro-Optics/Infrared Sensor Processing
Office of Naval Research
ONR Department Code: 312
875 North Randolph Street
Arlington, VA 22203-1995

Tel: (703) 696-5787
Fax: 703-696-1331
michael.d.duncan2@navy.mil

Principal Investigator and
Technical Point of Contact:

Gonzalo R. Arce, Charles Black Evans Professor
Department of Electrical and Computer Engineering
University of Delaware
Newark, DE 19716

Tel: (302) 831-1493
Fax: (302) 831-4316
arce@ece.udel.edu
www.ee.udel.edu/∼arce

Co-Principal Investigators:

Dennis W. Prather, College of Engineering Alumni Professor
Department of Electrical and Computer Engineering
University of Delaware
Newark, DE 19716

Tel: (302) 831-8170
Fax: (302) 831-4316
dprather@ee.udel.edu
www.ee.udel.edu/∼dprather

Javier Garcia-Frias, Professor
Department of Electrical and Computer Engineering
University of Delaware
Newark, DE 19716

Tel: (302) 831-0751
Fax: (302) 831-4316
jgarcia@ee.udel.edu
www.ee.udel.edu/∼jgarcia

Report Documentation Page

Form Approved
OMB No. 0704-0188

1. REPORT DATE	2. REPORT TYPE	3. DATES COVERED
15 JUL 2010		**00-00-2010 to 00-00-2010**

4. TITLE AND SUBTITLE	5a. CONTRACT NUMBER
Spectrally Adaptable Compressive Sensing Imaging System	5b. GRANT NUMBER
	5c. PROGRAM ELEMENT NUMBER
6. AUTHOR(S)	5d. PROJECT NUMBER
	5e. TASK NUMBER
	5f. WORK UNIT NUMBER
7. PERFORMING ORGANIZATION NAME(S) AND ADDRESS(ES) **Department of Electrical and Computer Engineering,University of Delaware,Newark,DE,19716**	8. PERFORMING ORGANIZATION REPORT NUMBER
9. SPONSORING/MONITORING AGENCY NAME(S) AND ADDRESS(ES)	10. SPONSOR/MONITOR'S ACRONYM(S)
	11. SPONSOR/MONITOR'S REPORT NUMBER(S)

12. DISTRIBUTION/AVAILABILITY STATEMENT
Approved for public release; distribution unlimited

13. SUPPLEMENTARY NOTES

14. ABSTRACT

15. SUBJECT TERMS

16. SECURITY CLASSIFICATION OF:			17. LIMITATION OF ABSTRACT	18. NUMBER OF PAGES	19a. NAME OF RESPONSIBLE PERSON
a. REPORT **unclassified**	b. ABSTRACT **unclassified**	c. THIS PAGE **unclassified**	**Same as Report (SAR)**	**11**	

In this effort we will design and develop a multi spectral sensing imaging and communications system based on a compressive sensing (CS) architecture that can computationally adapt dynamically, in real time, to a set of optimal spectral band(s) needed to address the desired tactical missions. The effort integrates the development and implementation of state of the art signal processing algorithms and communications, especially compressive sensing algorithms, with coded aperture multispectral sensors and optical design concepts, to attain a compact spectrally agile sensor system. The system under development is composed of three subsystems:

(1) Relay/dispersion and focal plane array (FPA) compressed measurements.

(2) Imaging and coded apertures.

(3) Analog source/channel coding subsystem. In this quarter, the following progress has been attained in each of these thrusts:

For the period of performance ending June 2010 the following has been accomplished under this contract in each of the subsystems:

1 Relay Compressed Measurements

1.1 Installed a monochromator-based setup to acquire calibration cubes needed by the image reconstruction algorithm

The goal of the proposed imager is to obtain information about the imaging scene by measuring the intensity of the light at each spatial location at different wavelengths which helps to obtain detailed information of the object. Thus, in this part of the effort, we installed an elaborate setup involving a monochromator along with other optical parts to acquire calibration cubes which could be used in the reconstruction of the image. The image reconstruction algorithm needs to be trained before being used in the image reconstruction experiment. The training process mainly involves the acquisition of a calibration cube, which is the a priori knowledge of the spatially shifted information of the photomask in different spectral channels. The calibration cube can be different when different lenses/prisms are used to build the system. To experimentally realize such a training process (acquiring the calibration cube), we built a spectrally adjustable illumination source using a monochromator and a Xenon (Xe) lamp. The monochromator used in our experiments is supplied by the Oriel Corporation (Oriel model number: 77200). Using suitable gratings and splits, this monochromator can achieve a spectral resolution of 1 nm. The output spectrum of the monochromator can be adjusted by rotating the blazing-grating in the monochromator. Thus, various spectrum ranges can be obtained with different gratings. For our monochromator, the spectrum-range is 440-670nm (visible). A Xe lamp (Newport model number: 66477) is used as the input to the monochromator. Figure 1 shows the monochromator setup.

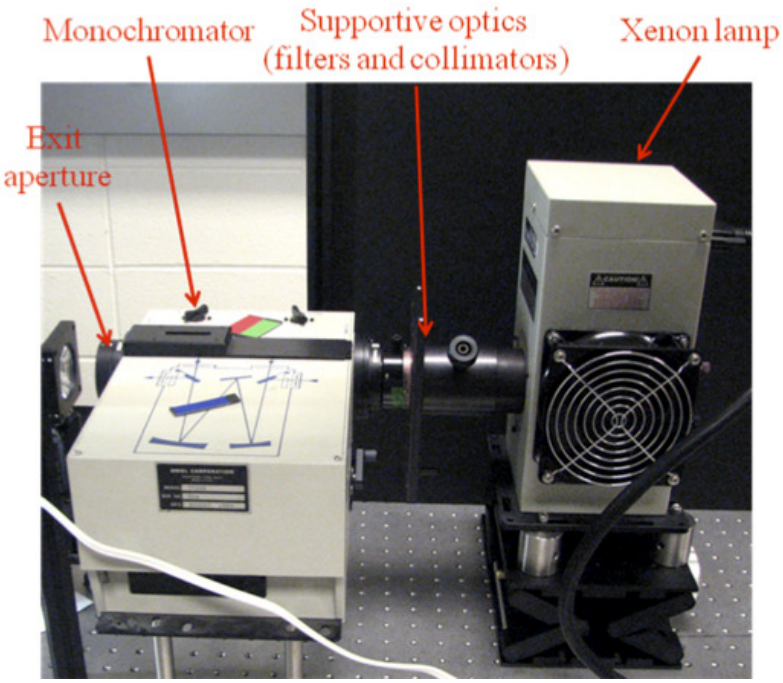

Figure 1: Monochromator setup. The output spectrum of the monochromator can be adjusted by rotating blazing-grating. The spectrum-range is 440-670nm (visible).

1.2 Acquisition of the calibration cube

The key components in the process of obtaining the calibration cube are the monochromator, photomask, prism, relay lens and a CCD camera. Particularly, the monochromator serves as the source; photomask is used for the random aperture code while the prism is used to introduce spectral dispersion. A relay lens relays the image from the plane of the coded aperture to the CCD which captures the dispersed image. Moreover, we used prisms of different apex angles to acquire the calibration cube, including an equilateral prism (Apex angle: 60), a right angle prisms (Apex angle: 45), a wedge prism (Apex angle: 18), and the double-amici prism mentioned in our last quarterly report in order to analyze their performances. Figure 2 shows the experimental setup used to acquire the calibration cube.

Figure 3 shows an example of a calibration cube obtained using the equilateral prism. The spectral resolution of the monochromator is 1nm. Therefore, for the given spectral range, there are 231 slices in the calibration cube. We show 21 of them in Fig. 3. The adjacent spectral images in this figure have a 10 nm difference in monochromator-emission wavelength.

In addition to equilateral prisms, we also used prisms with apex angles of 450 and 180 to acquire the calibration cube. In particular, Fig. 4 compares the calibration cubes obtained with different prisms. Generally speaking, the addition of prism introduces aberrations to the image formation process. For instance, we can see the edges of the calibration cubes have some curvatures. The aberrations are caused by the geometric shape of the prism. The prism has different thicknesses at different heights with respect to the apex angle. When the light propagates through the prism at different height/angle, its propagation will be affected

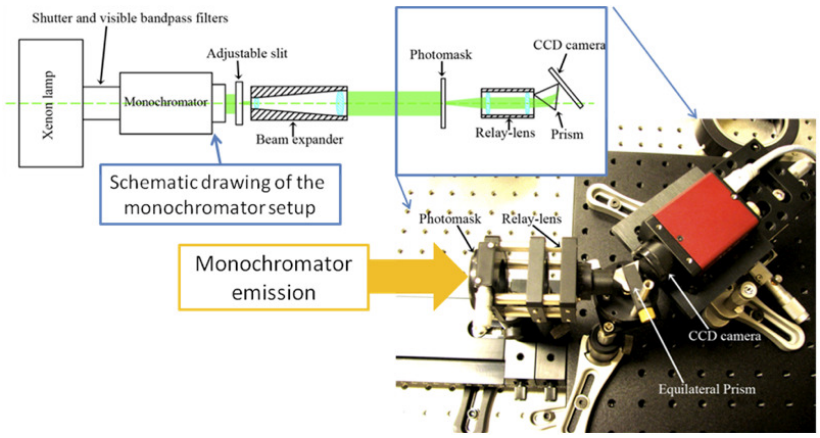

Figure 2: Experimental setup used to acquire the calibration cube using an equilateral prism with apex angle (apex angle: 60)

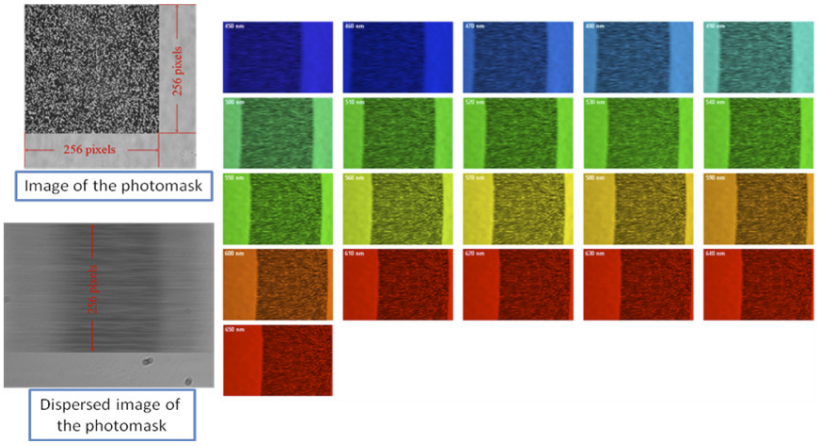

Figure 3: Calibration cube obtained using an equilateral prism (apex angle: 60).

by different thicknesses of the glass material. Since the aberrations are considered in the training process, the image reconstruction algorithm can minimize the quality degradation caused by the aberrations. In Fig. 4, we can see that calibration cubes acquired using prisms of smaller apex angles have apparently less field curvature.

2 Code Aperture Agile Spectral Imaging System (CAASI)

Recently, the Coded Aperture Snapshot Spectral Imaging (CASSI) architecture has made it possible to implement CS in spectral imaging. CASSI is indeed a remarkable imaging architecture that has been studied extensively in [1, 3, 4]. The single-shot CASSI architecture, however, may use excessive compression to represent spectrally rich image cubes under surveillance, leading in some cases to low quality image reconstructions as well as low spectral resolution. The coding and reconstruction algorithms in CASSI are also rigid because the entire spectral image cube is reconstructed at once. The new CAASI aims to overcome

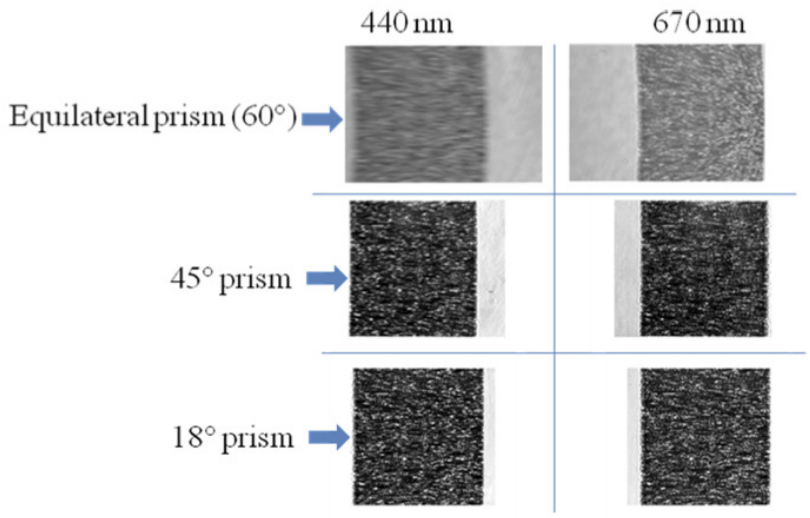

Figure 4: Calibration cubes obtained using the prisms of different apex angles.

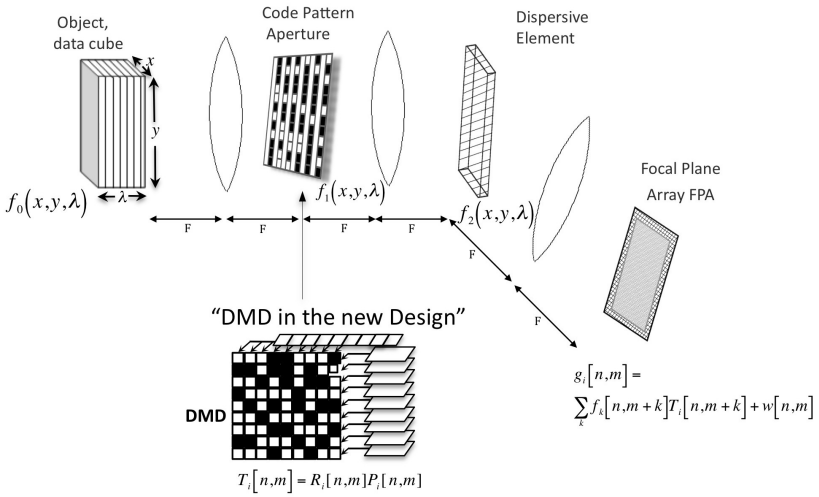

Figure 5: Representation of the CAASI parts. The fix code aperture in the traditional CASSI system is replaced by a spatial light modulator.

this difficulties and provides the flexibility to recover a specific subset of spectral bands with controllable SNR or reconstruction time.

The compressive code aperture single shot spectral imaging system is depicted in Fig. 5 [1]. The coding is realized by the coded aperture $T(x, y)$ as applied to the image source density $f_0(x, y; \lambda)$ where (x, y) are the spatial coordinates and λ is the wavelength resulting in the coded field $f_1(x, y, \lambda)$. The coded density is spectrally dispersed by a dispersive element before it impinges on the focal plane array (FPA) as $f_2(x, y, \lambda)$,

$$f_2(x, y, \lambda) = \int \int T(x', y') f_0(x', y', \lambda) h(x' - \alpha\lambda - x, y' - y) dx' dy' \tag{1}$$

where $T(x', y')$ is the transmission function representing the code aperture, $h(x' - \phi(\lambda) - x, y' -$

y) is the optical impulse response of the system, and $\alpha\lambda$ is the dispersion induced by the prism assuming a linear dispersion. The compressive measurements across the FPA are realized by the integration of the field $f_2(x, y, \lambda)$ over the detector's spectral range sensitivity. The source density can be written in discrete form as $(\mathbf{F}_k)_{nm}$ where n, m index the spatial coordinates, and k determines the k^{th} spectral plane. Following the mathematical model in [4], the coding is realized by an aperture pattern $(\mathbf{T})_{nm}$. The compressed sensing measurements at the focal plane array can be written in the following matrix form:

$$(\mathbf{G})_{nm} = \sum_{k=1}^{L} (\mathbf{F}_k)_{n,m+k} (\mathbf{T})_{n,m+k} + \omega_{n,m} \tag{2}$$

where ω_{nm} represents white noise, L is the number of spectral bands and where $n \in \{1, 2, ..., N\}$ and $m \in \{1, 2, ..., M\}$ index the pixels on the detector. The expression in (2) can be expressed as

$$\mathbf{g} = \mathbf{H}\mathbf{f} + \omega = \mathbf{H}\Psi\theta + \omega \tag{3}$$

where $\mathbf{g}$ and $\mathbf{f}$ are a vector representation of $\mathbf{G}$ and $\mathbf{F}$ respectively. $\mathbf{H}$ is the projection matrix, Ψ is a Kronecker basis representation, and θ is a sparse coefficient vector representing $\mathbf{f}$. If the aperture code pattern is fixed and only one snap-shot is detected, the resultant spectral imager is the so-called single disperser, or single-shot, CASSI architecture [2]. In this case, the entire 3-D multispectral image cube is compressed into a single 2-D compressive image measurement at the FPA. The compression factor η, defined as

$$\eta = 1 - \frac{M + L - 1}{M \times L}, \tag{4}$$

indicates the grade of compressive measurements. As $\eta \to 1$ the linear set of equations in (3) became severely underdetermined causing the CASSI measurements to be highly compressed, and in consequence the accurate reconstruction of the original information is difficult. On the contrary, as $\eta \to 0$ little compression is attained making it easier to recover the information embedded in $\mathbf{G}$. The spectral image cube $\mathbf{f}$ can be reconstructed by solving the optimization problem $\hat{\mathbf{f}} = \Psi\{\text{argmin}_{\theta'} \|\mathbf{G} - \mathbf{H}\Psi\theta'\|_2^2 + \tau\|\theta'\|_1\}$ where $\tau > 0$ is a regularization parameter that balances the conflicting tasks of minimizing the least square of the residuals while, at the same time, yielding a sparse solution[5]. In our work, we have obtained an equivalent model equation of CASSI system in alternative form as

$$\mathbf{g}_q = \mathbf{D}\mathbf{C}_q\mathbf{f}_q, \tag{5}$$

where $\mathbf{D}$ represents the operation of the dispersive element, and $\mathbf{C}_q$ is the matrix representation of the q^{th} row of the code aperture. The vector representation in (5) characterizing CASSI, will be very useful in our project.

3 Analog Source/channel Coding Subsystem

In this work, we use analog joint source-channel coding for the transmission of data samples at high rates. Here, we study the performance of such a system in comparison with optimized

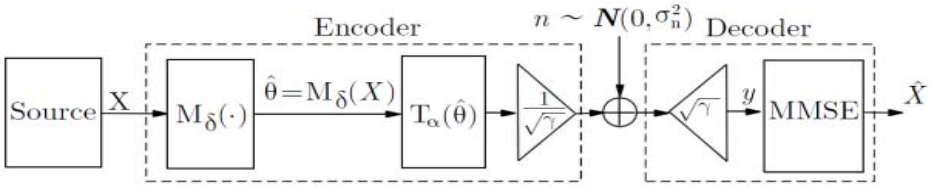

Figure 6: Block diagram of an N:1 bandwidth compression analog joint source-channel coded system.

capacity approaching digital Bit Interleaved Coded Modulation (BICM) schemes. The aim is to determine under which circumstances it is more convenient to use each communication setup. We measure the performance of both analog and digital systems in terms of Signal-to-Distortion Ratio (SDR) versus Channel Signal-to-Noise Ratio (CSNR) when Gaussian and Laplacian distributed sources are transmitted. Notice that Gaussian and Laplacian sources are of interest for reasons beyond their theoretical significance. In fact, images represented in transform domains (e.g., wavelets) can be accurately modeled using these distributions, which makes the analog joint source-channel coding system very relevant for image communications [12]. We show that analog transmission performs better than the digital scheme with a much lower encoding and decoding complexity.

3.1 Analog joint source-channel coded system

The distortion between source symbols $X = \{x_i\}_{i=1}^N$ and decoded symbols $\hat{X} = \{\hat{x}_i\}_{i=1}^N$ is calculated according to the MSE, defined as $MSE = \frac{1}{N}\sum_{i=1}^{N} ||x_i - \hat{x}_i||^2$. Consequently, the system performance can be measured in terms of the output SDR with respect to the CSNR, with SDR defined as SDR = 10 log (1/MSE), where the source symbols are normalized to unit mean power. Given N and K, the theoretival limit (OPTA) is calculated by equating the rate distortion function to the AWGN channel capacity [8]. For example, for Gaussian sources we have $N \log(1/MSE) = K \log(1 + 1/\sigma_n^2)$.

Figure 6 shows the block diagram of an N:1 analog joint source-channel coding system where the source generates blocks of B i.i.d. symbols that are encoded into B/N channel symbols. Without loss of generality, we assume a source distribution with zero mean and unit variance and also that the mean transmit power is equal to one. In this paper, we focus on memoryless Gaussian and Laplacian sources. A particular type of parameterized space-filling continuous curves, called spiral-like curves [8]-[10], can be used to encode the $X = (x1, x2)$ source samples. For the case of $2:1$ compression ($i.e., N = 2$), they are formally defined as

$$\begin{cases} x_{\theta,1} = sign(\theta)\frac{\triangle}{\pi} sin(\theta) \\ x_{\theta,2} = \frac{\triangle}{\pi} cos(\theta) \end{cases} \qquad for \;\; \theta \in \mathcal{R} \tag{6}$$

where $\triangle$ is the distance between two neighboring spiral arms, and θ is the angle from the origin to the point $X_\theta = (x_{1,v}, x_{2,v})$ on the curve. Therefore, each pair of source samples, x1 and x2, represent a specific point in $\mathcal{R}^2$ that is matched to the closest point $X_\theta = (x_{1,v}, x_{2,v})$

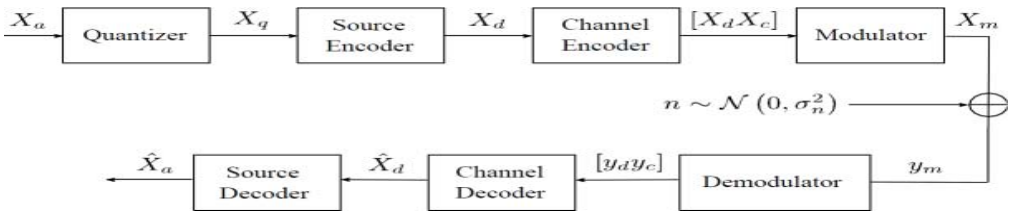

Figure 7: Block diagram of a Bit Interleaved Coded Modulation(BICM) system over AWGN channel.

on the spiral. The angle from the origin to that point on the spiral, $\hat{\theta}$, will be the channel symbol for x1 and x2, i.e.

$$\hat{\theta} = M_{\Delta}(X) = a \underset{\theta}{r} g \min \left\{ (x_1 \pm (\Delta/\pi)\theta \sin\theta)^2 + (x_2 - (\Delta/\pi)\theta\cos\theta)^2 \right\} \tag{7}$$

Since our goal is the minimization of the MSE, the bidimensional space has to be filled by the spiral in the best possible way for every CSNR value. On one hand, by changing the $\triangle$ value, we manage to optimize this matching and to improve the system performance. On the other hand, it is possible to achieve higher compression rates (i.e. N:1) by extending (1) to generate more complex curves [14], [15].

The next step consists in defining an invertible function of $\hat{\theta}$-with the corresponding normalization factor to ensure the transmit power constraint. In [8, 10, 16] the invertible function $T_\alpha(\hat{\theta}) = \hat{\theta}^\alpha$ with $\alpha = 2$, was proposed. However, as shown in [11], the system performance can be improved if α and $\triangle$ are numerically optimized for each different CSNR value. Therefore, the channel symbol is $T_\alpha\left(\hat{\theta}\right)/\sqrt{\gamma}$, where $\sqrt{\gamma}$ is the normalization factor. In summary, the received symbol y at the decoder can be expressed as $y = T_\alpha(M_\Delta(X)) + n\sqrt{\gamma}$, where n is Gaussian noise. Given a received symbol y, MMSE decoding is performed at the receiver to calculate an estimation of the corresponding source symbol. Optimal MMSE decoding can be expressed as

$$\hat{X}_{MMSE} = E\{X|y\} = \int X p(X|y)\, dX = (1/p(y)) \int X p(y|X)\, p(X)\, dX \tag{8}$$

where the mapping function $M_\Delta(\cdot)$ is used to obtain the conditional probability $p(y|X)$. Note that the integral in (8) can only be calculated numerically because $M_\Delta(\cdot)$ is discontinuous and highly non-linear. To do so, X is first discretized using a uniform step and a mapped value is calculated for each discretized point according to (7). As a result, we obtain a discretized version of $p(y|X)$. Next, $p(X)$ is also computed for each point, and thus the calculation of the integral is reduced to multiplicative and additive operations. Since this discretization does not depend on the received symbol, it is calculated once off-line and stored in the decoder. Although in this paper we focus on 2:1 systems, the proposed system can be readily modified to adapt the compression rate from N:1 to N:K [17].

3.2 Bit interleaved coded modulation (BICM)

Figure 7 shows the block diagram of a digital BICM system. We assume a discrete-time source that produces Gaussian and Laplacian independent and identically distributed (i.i.d.)

real valued analog symbols Xa. These continuous samples are mapped to a discrete set of values using an optimum Q-level scalar quantizer. Both, the quantization levels and the partition regions can be obtained using the well-known Lloyd-Max algorithm [21, 22]. Although better performance could be obtained with vector quantization, we discarded this possibility to keep the overall quantizing complexity at a low level. Next, the quantized discrete-time symbols are converted into a binary representation using a suitable source encoder. Again, among the many existing source encoding methods, we decided to use Huffman encoding because it is a simple algorithm and approaches the source entropy. The input alphabet to the Huffman encoder is made up of the Q-levels of the scalar quantizer, i.e., no grouping is performed prior to the encoding. The length of the average Huffman codeword used to represent each source sample will be denoted by Lm. The output bit sequence is encoded with a rate r capacity approaching channel encoder. Due to their low encoding and decoding complexity, we decided to use Irregular Repeat Accumulate (IRA) codes [23]. Finally, the channel encoded bits are modulated using a real-valued M-PAM constellation. Notice that an interleaver between the channel encoder and the modulator is not strictly necessary since we are transmitting over an AWGN channel. A one-dimensional PAM constellation has been chosen to keep the same signaling as the analog system in Section II where real analog encoded symbols are transmitted. The constellation size M limits the maximum attainable data rate over the channel. We chose the value M = 256 which allows the transmission of a maximum of 8 bits per channel use, a transmission rate high enough for the comparison carried out in the ensuing section. Higher values of M could be used but they yield to extremely complex PAM constellations that are not feasible in practice. At the receiver, an optimum detector calculates the LLRs of the transmitted bits and passes them to the sum-product IRA decoding algorithm. After a maximum number of decoding iterations, the resulting bits are hard-decoded and dequantized to the corresponding levels.

References

[1] A. Wagadarikar, R. John, R. Willett, and D. Brady, *Single disperser design for coded aperture snapshot spectral imaging*. Appl. Opt. 47, B44-B51 (2008).

[2] D. J. Brady, *Optical Imaging and Spectroscopy*. Address:Wiley, John and Sons, 2009.

[3] A. Wagadarikar and R. John and R. Willett and D. Brady, "Imaging systems; Spectrometers and spectroscopic instrumentation; Spectrometers," *Appl. Opt.*, vol. 47, pp. B44-B51, 2008.

[4] A. Wagadarikar and N. P. Pitsianis and X. Sun and D. J. Brady, "Video rate spectral imaging using a coded aperture snapshot spectral imager," *Opt. Express*, vol. 17, pp. 6368-6388, 2009.

[5] S. J. Kim and K. Koh and M. Lustig and S. Boyd and D. Gorinevsky, "An Interior-Point Method for Large-Scale l1_Regularized Least Squares," *IEEE Journal of Selected Topics in Signal Processing*, vol. 1, pp. 606-617, 2007.

[6] C. E. Shannon, A mathematical theory of communication (part I), Bell System Technical Journal, vol. 27, pp. 379-423, 1948.

[7] T. J. Goblick, Theoretical limitations on the transmission of data from analog sources, IEEE Trans. Inf. Theory, vol. 11, no. 4, pp. 558-567, Oct. 1965.

[8] S. Y. Chung, On the construction of some capacity-approaching coding schemes, Ph.D. dissertation, Dept. EECS, Massachusetts Institute of Technology, 2000.

[9] T. A. Ramstad, Shannon mappings for robust communication, Telektronikk, vol. 98, no. 1, pp. 114-128, 2002.

[10] G. E. Oien, F. Hekland, and T. A. Ramstad, Using 2:1 shannon mapping for joint source-channel coding, in Proc. DCC05, Mar. 2005.

[11] Y. Hu, J. Garcia-Frias, and M. Lamarca, Analog joint source-channel coding using space-filling curves and MMSE decoding, in Proc. DCC09, Mar. 2009.

[12] Y. Hu, J. Garcia-Frias, and G. R. Arce, Non-linear coding for improved performance in compressed sensing, in Proc. CISS09, Mar. 2009.

[13] T. Berger and D. Tufts, Optimum pulse amplitude modulation-I: transmitter-receiver design and bounds from information theory, IEEE Trans. Inf. Theory, vol. 13, no. 2, pp. 196-208, Apr. 1967.

[14] P. A. Floor and T. A. Ramstad, Dimension reducing mappings in joint source-channel coding, in Proc. NORSIG, Jun. 2006.

[15] P. A. Floor, On the theory of shannon-kotelnikov mappings in joint source-channel coding, Ph.D. dissertation, Norwegian University of Science and Technology, 2008.

[16] P. A. Floor, F. Hekland, and T. A. Ramstad, Shannon-Kotelnikov mappings in joint source-channel coding, IEEE Trans. Commun., vol. 57, no. 1, pp. 95-104, Jan. 2009.

[17] Y. Hu, J. Garcia-Frias, and M. Lamarca, MMSE decoding for analog joint source channel coding using Monte Carlo importance sampling, in Proc. SPAWC09, Jun. 2009.

[18] G. Ungerboeck, Channel coding with multilevel/phase signals, IEEE Trans. Inf. Theory, vol. IT-28, pp. 56-67, Jan. 1982.

[19] E. Zehavi, 8-PSK trellis codes for a rayleigh channel, IEEE Trans. Commun., vol. 40, pp. 873-884, May 1992.

[20] G. Caire, G. Taricco, and E. Biglieri, Bit-interleaved coded modulation, in ICC (3), 1997, pp. 1463-1467.

[21] S. P. Lloyd, Least squares quantization in PCM, IEEE Trans. Inf. Theory, vol. IT-28, no. 2, pp. 129-137, Mar. 1982.

[22] J. Max, Quantizing for minimum distorsion, IEEE Trans. Inf. Theory, vol. IT-6, pp. 7-12, 1960.

[23] H. Jin, A. Khandekar, and R. J. McEliece, Irregular repeat-accumulate codes, in Proc. 2nd Int. Symp. Turbo Codes and Related Topics, Brest, France, Sep. 2000, pp. 1-8.

[24] S. ten Brink and G. Kramer, Design of Repeat-Accumulate codes for iterative detection and decoding, IEEE Trans. Signal Process., vol. 51, no. 11, pp. 2764-2772, Nov. 2003.